The effect of 1H offset and flip-angle on heteronuclear decoupling efficiency in ROSPAC pulsed sequence: A Floquet description

Journal Article

Author(s):
Simion, Andrea; Ernst, Matthias (iD); Filip, Claudiu

The effect of ¹H offset and flip-angle on heteronuclear decoupling efficiency in ROSPAC pulsed sequence: A Floquet description

View Online   Export Citation   CrossMark

Andrea Simion,[1,2] (ID) Matthias Ernst,[3,a] (ID) and Claudiu Filip[1] (ID)

AFFILIATIONS

[1] National Institute for Research and Development of Isotopic and Molecular Technologies, 400293 Cluj-Napoca, Romania
[2] Faculty of Physics, Babes-Bolyai University, 400084 Cluj-Napoca, Romania
[3] Physical Chemistry, ETH Zurich, CH-8093 Zurich, Switzerland

[a] Author to whom correspondence should be addressed: maer@ethz.ch

ABSTRACT

A new heteronuclear decoupling sequence for solid-state NMR and magic angle spinning faster than 60 kHz was recently introduced [Simion *et al.*, J. Chem. Phys. **157**, 014202 (2022)]. It was dubbed ROtor-Synchronized Phase-Alternated Cycles (ROSPAC), and it offers robustness for a large range of chemical shifts and low radio-frequency (RF) powers and is almost independent of the radio-frequency power. Here, we theoretically explore the robustness of the ROSPAC sequence toward ¹H offset and RF field inhomogeneities, as well as the spacing effect of the π pulses on the decoupling efficiency. We use a generalized theoretical framework based on the Floquet theory to assess these parameters. The optimum decoupling conditions, where the magnitude of the second-order cross-terms and first-order resonance conditions are small, were identified.

I. INTRODUCTION

Efficient averaging of isotropic and anisotropic interactions is a prerequisite to achieving high spectral resolution and sensitivity in solid-state NMR. This is typically implemented by simultaneously spinning the sample about the magic angle (MAS) and radio-frequency (RF) irradiation on the non-observed nuclei. The latter allows decoupling abundant nuclei (often ¹H) from the dilute, observed nucleus (often ¹³C or ¹⁵N) and is called heteronuclear spin decoupling.[1,2] Heteronuclear decoupling works best if either the nutation frequency of the rf field is much larger or much smaller (typically by at least a factor of 3 in both directions) than the MAS frequency. If the two frequencies are in the same range, rotary-resonance recoupling conditions can lead to a recoupling of the heteronuclear dipolar interactions, severely reducing the performance of the heteronuclear decoupling sequences.[3–5]

Improving the efficiency of spin decoupling is a subject of continued interest in solid-state NMR, especially with the recent developments in instrumentation, e.g., fast spinning frequencies (> 100 kHz)[6,7] and high magnetic fields (up to 35.2 T).[8–10] As a consequence of these instrumental advances, a wide range of new or improved applications has become possible.[7,11,12] Heteronuclear decoupling sequences contain a series of pulses modulated by the amplitude, frequency, or phase.[1,2,6,7,13–19] To avoid resonance conditions, the basic building block is often short but can then be expanded using approaches such as super cycling of the basic block,[20] incorporation of refocusing π-pulses,[21] and non-rotor-synchronized[22] or rotor-synchronized schemes.[23,24]

For decoupling at high MAS frequencies ($\nu_r \gtrsim 60$ kHz), low-power irradiation is preferred, leading to a reversal of the averaging processes compared with high-power decoupling. Low-power decoupling was first implemented using continuous-wave

(CW) type sequences[25] but later extended to more complex sequences like WALTZ,[26,27] two-pulse phase-modulated decoupling (TPPM),[29] swept-frequency TPPM (sw-TPPM),[14] small phase incremental alternation (SPINAL),[29] and X inverse X (XiX)[15,30] and its variants.[13,21]

Recently, a new low-power heteronuclear decoupling pulse sequence for MAS faster than 60 kHz dubbed ROtor-Synchronized Phase-Alternated Cycles (ROSPAC) was introduced,[24] being an improved version of the RS-HEPT sequence.[23,31] It is a phase-modulated sequence, containing 16 π-pulses spaced by n rotor periods ($n\tau_r$) (see Fig. 1). It has a low-duty cycle in the pulsed decoupling regime, and only the pulse lengths require optimization. It was found by numerical simulations, and experimental measurements that the delay between the π-pulses ($n\tau_r$) should be selected based on the spinning frequency to avoid rotary-resonance (R^3) recoupling conditions and obtain a sequence that is almost independent of the RF power. Moreover, it was demonstrated that the sequence is very robust against ^{1}H offset at fast spinning frequencies (100 kHz). However, there is not yet a theoretical description of the sequence, which would explain this behavior. Such a theoretical understanding would also allow further optimization to obtain the best decoupling efficiency and propose further improvements.

Here, we use a generalized theoretical framework based on Floquet theory[32] to investigate the robustness of the ROSPAC sequence toward ^{1}H offset and RF field inhomogeneities, as well as the effect of the spacing of the pulses on the decoupling efficiency. Numerical calculations based on analytical solutions were done for three spinning frequencies, 100, 60, and 40 kHz, and three decoupling regimes, low-power, intermediate-power, and high-power decoupling, i.e., at ^{1}H nutation frequencies of 20, 70, and 160 kHz, respectively. The non-resonant second-order effective Hamiltonians that characterize the residual couplings arising from cross-terms between heteronuclear dipolar couplings and chemical shift anisotropy (CSA) tensors and from cross-terms between heteronuclear and homonuclear dipolar couplings under MAS were evaluated. Their scaling factors were obtained from the interaction-frame
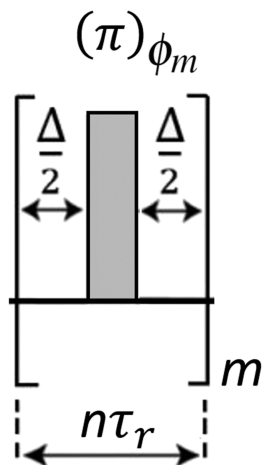
trajectory. In addition, the magnitude of the first-order resonance conditions was calculated. The optimum decoupling conditions and further improvements are discussed.

II. THEORY

We consider a system of N abundant I spins (e.g., ^{1}H) that are coupled to a rare S spin (e.g., ^{13}C). In the usual rotating frame (rotating with the Larmor frequency around the z-axis), the spin-system Hamiltonian under MAS is given by

$$\hat{H}(t) = \sum_{n=-2}^{2} \omega_S^{(n)} \hat{S}_z e^{in\omega_r t} + \sum_{k=1}^{N}\sum_{n=-2}^{2} \omega_k^{(n)} \hat{I}_{kz} e^{in\omega_r t}$$
$$+ \sum_{k=1}^{N}\sum_{n=-2}^{2} \omega_{Sk}^{(n)} 2\hat{S}_z \hat{I}_{kz} e^{in\omega_r t}$$
$$+ \sum_{k<l}\sum_{\substack{n=-2,\\n\neq 0}}^{2} \omega_{kl}^{(n)} (3\hat{I}_{kz}\hat{I}_{lz} - \hat{\vec{I}}_k \cdot \hat{\vec{I}}_l) e^{in\omega_r t} + \hat{H}_{RF}(t), \quad (1)$$

where $\omega_S^{(n)}$ and $\omega_k^{(n)}$ represent the spatial components of the chemical-shift tensors for the S and I spins, respectively, whereas $\omega_{Sk}^{(n)}$ and $\omega_{kl}^{(n)}$ are the Fourier coefficients of the heteronuclear and homonuclear dipolar couplings.[32] The last term represents the radio-frequency (RF) Hamiltonian, which, for periodic irradiation, has the general form,

$$\hat{H}_{RF}(t) = \omega_1(t)\sum_{k=1}^{N} (\cos(\phi(t))\hat{I}_{kx} + \sin(\phi(t))\hat{I}_{ky}), \quad (2)$$

where $\phi(t)$ is the phase of the applied pulse and $\omega_1(t)$ is the RF amplitude.

A. On-resonant and off-resonant irradiation

To analyze the efficiency of decoupling sequences, it is often convenient to transform the spin-system Hamiltonian of Eq. (1) into an interaction frame with the radio-frequency Hamiltonian. The most general case is off-resonance irradiation of the spins where we use the combined offset and rf-field Hamiltonian for the interaction-frame transformation:

$$\hat{\tilde{H}}(t) = \hat{U}_1(t)\hat{H}(t)\hat{U}_1^{-1}(t), \quad (3)$$

where the tilde indicates that the Hamiltonian is in the interaction frame and $\hat{U}_1(t)$ is given by

$$\hat{U}_1(t) = \hat{T}\exp\left(-i\int_0^t \left(\hat{H}_{RF}(t_1) + \Delta\Omega\sum_{k=1}^{N}\hat{I}_{kz}\right)dt_1\right), \quad (4)$$

during pulses and by $\hat{U}_1(t) = \hat{\mathbf{1}}$ during the delays between pulses. Here, $\hat{T}$ is the Dyson time-ordering operator.

FIG. 1. Schematic of the ROSPAC heteronuclear decoupling sequence. The $m = 16$ π pulses are spaced by n rotor cycles and have phases $\phi_m = \{10, 350, 15, 345, 20, 340, 15, 345, 350, 10, 345, 15, 340, 20, 345, 15\}$.

The spin operators in the interaction frame can be represented as a linear combination of the three Cartesian spin operators in the laboratory frame with time-dependent coefficients:[33]

$$\hat{\tilde{I}}_z(t) = a_x(t)\hat{I}_x + a_y(t)\hat{I}_y + a_z(t)\hat{I}_z, \tag{5}$$

where the time-dependent coefficients $a_\chi(t)$, with χ = x, y, and z represent the spin-trajectory coefficients under the interaction-frame transformation. In general, they can be expressed as a Fourier series with the two frequencies ω_m and ω_{eff} as[33]

$$a_\chi(t) = \sum_{k=-\infty}^{\infty} \sum_{l=-1}^{1} a_\chi^{(k,l)} e^{ik\omega_m t} e^{il\omega_{eff} t}, \tag{6}$$

where k and l are integer numbers, and $a_\chi^{(k,l)}$ are the Fourier coefficient characterizing the interaction-frame trajectory of the $\hat{\tilde{I}}_z(t)$ operator.

B. Effective Hamiltonian and second-order cross-terms

In the general case, the time-dependent interaction-frame Hamiltonian $\hat{\tilde{H}}(t)$ is, therefore, modulated by three basic frequencies, namely the MAS frequency ω_r, the modulation frequency $\omega_m = 2\pi/(16n\tau_r)$ (see. Fig. 1), and the effective nutation frequency ω_{eff}, and is given by

$$\hat{\tilde{H}}(t) = \sum_{n=-2}^{2} \sum_{k=-\infty}^{\infty} \sum_{l=-2}^{2} \hat{\tilde{H}}^{(n,k,l)} e^{in\omega_r t} e^{ik\omega_m t} e^{il\omega_{eff} t}, \tag{7}$$

where $\hat{\tilde{H}}^{(n,k,l)}$ are the Fourier coefficients of the time-dependent interaction-frame Hamiltonian. To characterize decoupling, the residual couplings under decoupling are the most important terms that are contained in the non-resonant part of the effective Hamiltonian. The non-resonant part of the effective Hamiltonian is given by

$$\hat{\bar{H}} = \hat{\bar{H}}^{(1)} + \hat{\bar{H}}^{(2)} + \cdots = \hat{\bar{H}}^{(0,0,0)} + \hat{\bar{H}}^{(0,0,0)}_{(2)} + \cdots$$
$$= \hat{\bar{H}}^{(0,0,0)} - \frac{1}{2} \sum_{\nu,k,\lambda} \frac{\left[\hat{\tilde{H}}^{(-\nu,-k,-\lambda)}, \hat{\tilde{H}}^{(\nu,k,\lambda)}\right]}{\nu\omega_r + \kappa\omega_m + \lambda\omega_{eff}}. \tag{8}$$

The first-order contribution would only contain the homonuclear J couplings of the protons for on-resonance irradiation and, in addition, scaled heteronuclear J couplings and chemical shifts of the protons for off-resonance irradiation. Those terms will be neglected in the discussion since they are typically quite small. The second-order term determines the performance of the decoupling sequences, being directly responsible for the main contribution to the residual linewidth. One can decompose this non-resonant second-order term into six contributions,[32]

$$\hat{\bar{H}}^{(2)} = -\frac{1}{2} \sum_{\nu,k,\lambda} \frac{\left[\hat{\tilde{H}}^{(-\nu,-\kappa,-\lambda)}, \hat{\tilde{H}}^{(\nu,\kappa,\lambda)}\right]}{\nu\omega_r + \kappa\omega_m + \lambda\omega_{eff}}$$
$$= \hat{\bar{H}}_{IS\otimes I} + \hat{\bar{H}}_{IS\otimes II} + \hat{\bar{H}}_{I\otimes II} + \hat{\bar{H}}_{II\otimes II} + \hat{\bar{H}}_{I\otimes I} + \hat{\bar{H}}_{IS\otimes IS}, \tag{9}$$

where $\hat{\bar{H}}_{IS\otimes I}$ is the cross-term between the heteronuclear dipolar coupling and the I-spin CSA tensor and $\hat{\bar{H}}_{IS\otimes II}$ represent the cross-term between the heteronuclear and homonuclear dipolar couplings. These two terms directly influence the residual coupling under the decoupling sequence. The next two terms, $\hat{\bar{H}}_{I\otimes II}$ and $\hat{\bar{H}}_{II\otimes II}$, represent the cross-term between CSA tensor and homonuclear coupling, and the cross-term between homonuclear couplings of I-spins, respectively, and can have an effect on the I-spins diffusion, depending on the spinning frequency. The last two terms, $\hat{\bar{H}}_{I\otimes I}$ and $\hat{\bar{H}}_{IS\otimes IS}$, are cross terms between CSA and heteronuclear dipolar couplings, respectively, generating only fictitious fields that do not influence directly the residual line broadening but could have truncation effects in the Hamiltonian. The first two second-order terms are given by[32]

$$\hat{\bar{H}}_{IS\otimes I} = \sum_k \sum_{\nu=-2}^{2} \sum_{\chi=x,y,z} i\hat{S}_z \hat{I}_{k\chi} q_\chi^{(\nu)} \left(\omega_{kS}^{(-\nu)}\omega_k^{(\nu)} + \omega_{kS}^{(\nu)}\omega_k^{(-\nu)}\right), \tag{10}$$

$$\hat{\bar{H}}_{IS\otimes II} = \sum_{k\neq l} \sum_{\nu=-2}^{2} \sum_{\mu,\chi=x,y,z} -3i\hat{S}_z \hat{I}_{k\mu}\hat{I}_{l\chi} \left[q_{\mu\chi}^{(\nu)}\omega_{kS}^{(-\nu)}\omega_{kl}^{(\nu)} \right.$$
$$\left. - \left(q_{\mu\chi}^{(\nu)}\right)^* \omega_{kS}^{(\nu)}\omega_{kl}^{(-\nu)} \right], \tag{11}$$

where the scaling factors $q_\chi^{(\nu)}$ and $q_{\mu\chi}^{(\nu)}$ are given by

$$q_\chi^{(\nu)} = \sum_k \sum_{\lambda=-1}^{1} \frac{\varepsilon_{\chi ij} a_j^{(-\kappa,-\lambda)} a_i^{(\kappa,\lambda)}}{\nu\omega_r + \kappa\omega_m + \lambda\omega_{eff}}$$
$$q_{\mu\chi}^{(\nu)} = \sum_k \sum_{\lambda=-1}^{1} \frac{\varepsilon_{\chi ij} a_j^{(-\kappa,-\lambda)} a_{\chi i}^{(\kappa,\lambda)}}{\nu\omega_r + \kappa\omega_m + \lambda\omega_{eff}}. \tag{12}$$

Here, $\varepsilon_{\chi ij}$ is the Levi-Cività symbol and $a_{\mu\chi}^{(\kappa,\lambda)}$ are the Fourier coefficients for the rank-two spin tensor defined as a convolution of the rank-one Fourier coefficients $a_\chi^{(\kappa,\lambda)}$ [Eq. (6)] obtained from the interaction-frame trajectory.[32] Note that the two expressions in Eq. (12) are similar, except for the Fourier coefficients in the numerator, i.e., the former has a rank-one spin tensor ($a_i^{(\kappa,\lambda)}$), whereas the later has a rank-two spin tensor ($a_{\chi i}^{(\kappa,\lambda)}$). The two terms from the second-order non-resonant effective Hamiltonian [Eqs. (10) and (11)] lead to a direct residual line broadening of the S-spin. Their effect will be further analyzed for on-resonant and off-resonant irradiation. For this purpose, two scaling factors based on Eq. (12) will be calculated for ν = 1 and ν = 2 $\left(q_{IS\otimes I}^{(\nu)} = \sqrt{\sum_\chi \left(q_\chi^{(\nu)}\right)^2}\right.$ and $q_{IS\otimes II}^{(\nu)} = \sqrt{\sum_{\chi,\mu} \left(q_{\chi,\mu}^{(\nu)}\right)^2}\right)$, taking into account that for the ROSPAC sequence ω_{eff} = 0 for on-resonant irradiation (and $\omega_{eff} \neq 0$ otherwise). Note that for off-resonance irradiation the offset added to the RF Hamiltonian changes only the effective nutation frequency $\omega_{eff}(\Delta\Omega)$ and the Fourier coefficients $a_\chi^{(k,l)}$ as a function of offset, but the general equations obtained for the effective Hamiltonians [Eqs. (10) and (11)], and the scaling factors [Eq. (12)] are unchanged. The modulation frequency ω_m of the sequence is unchanged because the timing is unchanged.

C. First-order resonance conditions

We also analyze possible resonance conditions, since they could recouple different interactions that possibly lead to a line broadening. A first type of resonance condition is given by $n_0\omega_r + k_0\omega_m = 0$ since the sequence is always rotor synchronized. The modulation frequency $\omega_m = 2\pi/\tau_m$ is given by the number of rotor periods that the sequence spans as $\omega_m = \omega_r/(16n)$ or $\tau_m = 16n\tau_r$ (see Fig. 1). The strength of the resonance condition is directly given by the Fourier coefficients $a_\chi^{(16n,0)}$. As a measure for the strength of the resonance condition, we use the $a^{(k_0,0)} = \sqrt{\sum_\chi (a_\chi^{(k_0,0)})^2}$ parameter. Two other types of possible resonance conditions are $k_0\omega_m + l_0\omega_{eff} = 0$ and $n_0\omega_r + k_0\omega_m + l_0\omega_{eff} = 0$, but these are not of interest here because the former one can only be fulfilled for terms that are not modulated by MAS (i.e., $n_0 = 0$), meaning that only isotropic interactions could contribute to such a resonance condition, whereas the latter is never fulfilled because ω_{eff} is always smaller than $\frac{1}{2}\omega_m$ and ω_r is an integer multiple of ω_m. In the case of very small values of ω_{eff}, near-resonance conditions could become important, but they are difficult to describe by Floquet theory.
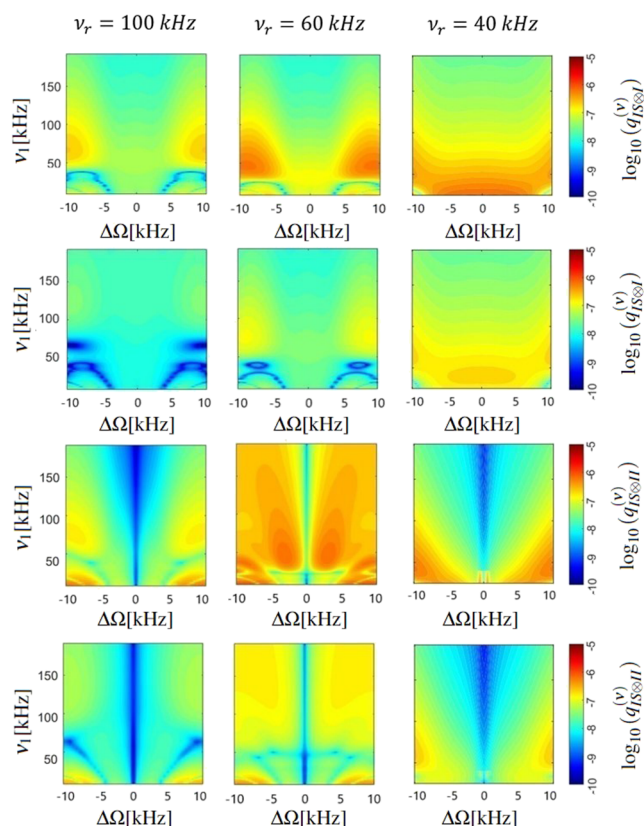
III. MATERIALS AND METHODS

The calculation of the interaction-frame trajectory, the Fourier coefficients, the cross-terms between the heteronuclear dipolar coupling and the I-spin CSA tensor and between the heteronuclear and homonuclear dipolar couplings, as well as the first-order resonance conditions, was done using the software package Matlab (The MathWorks Inc., Natick, MA, U.S.A.).

First, the interaction-frame trajectory under the ROSPAC sequence was obtained for the $\hat{I}_z$ operator at a given MAS frequency and different RF powers (supplementary material, Fig. S1). The spacing of the π pulses was set to $6\tau_r$ for $\nu_r = 100$ kHz, $4\tau_r$ for $\nu_r = 60$ kHz, and τ_r for $\nu_r = 40$ kHz, unless mentioned otherwise. Only the z-component of the I spin was considered because the Hamiltonian contains just z-components.

Second, the Fourier coefficients $a_\chi^{(k,l)}$ characterizing the interaction frame trajectories from Fig. S1 were obtained by a Fourier transform of the interaction-frame trajectory (supplementary material, Fig. S2). For low-power decoupling, i.e., 20 kHz, the number of the Fourier coefficients that have a contribution to the effective Hamiltonian correspond to low k-orders, i.e., for $k > 50$, they are small and were neglected. For intermediate-power or high-power decoupling, i.e., 70 and 160 kHz, respectively, the
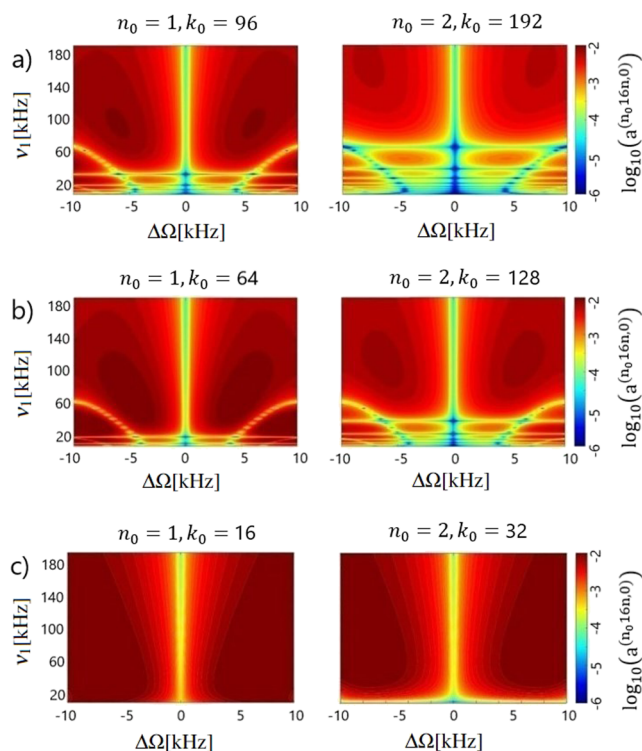
FIG. 2. Magnitude of the second-order cross-terms $[\log_{10}(q_{IS\otimes I}^{(\nu)})$ and $\log_{10}(q_{IS\otimes II}^{(\nu)})]$ as a function of the nutation frequency and ^{1}H offset for a rotation frequency of 100, 60, and 40 kHz, respectively.

FIG. 3. Magnitude of the Fourier coefficients $(\log_{10}(a^{(n_0 16n,0)}))$ at the $n_0\omega_r + k_0\omega_m = 0$ resonance conditions for $n_0 = 1$ and $n_0 = 2$, as a function of the nutation frequency and ^{1}H offset, for a rotation frequency of 100 kHz (a), 60 kHz (b), and 40 kHz (c), respectively.

magnitude of high k-orders increased and was considered, up to $k = 200$.

Experimental measurements were performed on a sample of labeled $^{13}C_2$–^{15}N-glycine ethyl ester, using a Bruker 0.7 mm triple-resonance MAS probe on a Bruker Avance-III 850 MHz spectrometer. A spinning frequency of 100 kHz was used in all experiments with a stability of about ±10 Hz. ^{13}C MAS NMR spectra were acquired using cross-polarization from protons with a linear ramp. The contact time was 1 ms with rf-field amplitudes of 70 and 30 kHz on ^{1}H and ^{13}C, respectively. For each spectrum, 16 scans with 2048 complex data points were acquired with a spectral width of 50 kHz and a recycle delay of 3 s. For decoupling using the ROSPAC sequence, a pulse with a flip angle β was applied every six rotor cycles without any active synchronization of the MAS frequency. The rf-field amplitude of the decoupling pulse was set to 20, 40, 80, and 160 kHz, respectively, using a simple 180° pulse to determine the power levels.

IV. RESULTS AND DISCUSSION

The theoretical results are divided into two main parts: (i) robustness toward ^{1}H offset and (ii) dependence of the decoupling performance on the flip angle. The former determines the quality of the decoupling under realistic conditions (e.g., a distribution of chemical-shift values of the protons), whereas the latter is related to the stability of the sequence and ease of setup (e.g., inhomogeneous RF fields and missetting of the rf-field amplitude).

A. Robustness toward ^{1}H offset
1. ^{1}H offset dependence on the spinning frequency and RF amplitude

The dependence of the decoupling efficiency on the chemical shift offset is one of the most important criteria for decoupling sequences. In liquid-state NMR, very good offset compensation at
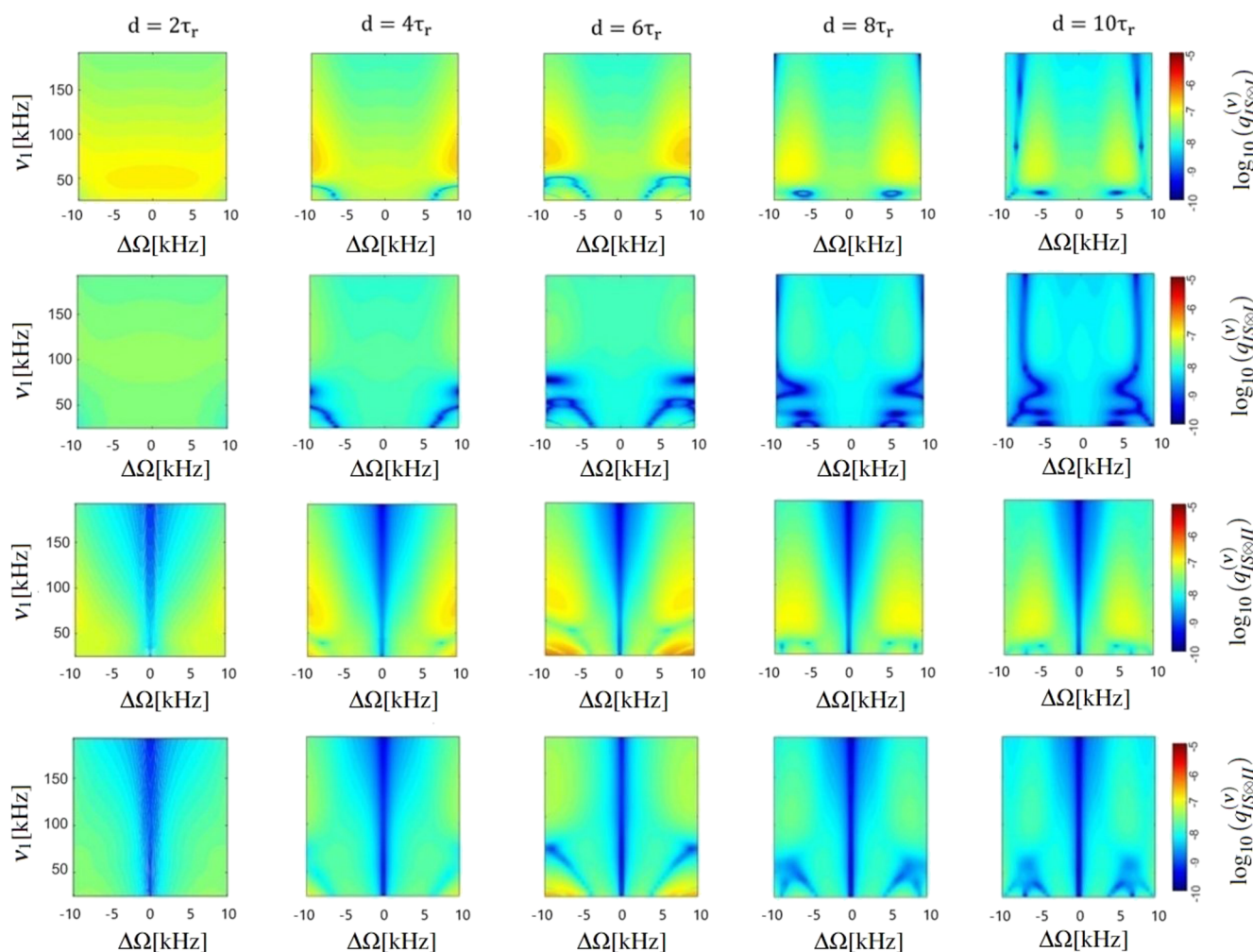
FIG. 4. Magnitude of the second-order cross terms [$\log_{10}(q_{IS\otimes I}^{(v)})$ and $\log_{10}(q_{IS\otimes II}^{(v)})$] as a function of the nutation frequency and ^{1}H offset for 100 kHz rotation frequency and different delays between the π-pulses.

the lowest possible field is one of the design features of the most commonly used decoupling sequences. In solid-state NMR, high-power decoupling sequences (i.e., $\omega_1 > 3\omega_r$) are usually inherently broadband enough since nutation frequency of the rf-field is about an order of magnitude larger than the chemical-shift range for protons. For low-power decoupling (i.e., $\omega_1 < \frac{1}{3}\omega_r$), however, the nutation frequency of the decoupling field is significantly smaller than the MAS frequency and is often in the same order of magnitude as the chemical-shift range of protons. Therefore, the chemical-shift offset dependence becomes an important parameter for these sequences.

Figure 2 shows the logarithm of the magnitude of the scaling factors [$\log_{10}(q_{IS\otimes I}^{(v)})$ and $\log_{10}(q_{IS\otimes II}^{(v)})$] for the second-order cross terms as a function of the RF amplitude (v_1) and ^{1}H offset frequency ($\Delta\Omega$), for three MAS frequencies: 100, 60, and 40 kHz. One can observe that the $v = 1$ cross term has a slightly higher contribution to the effective Hamiltonian than the $v = 2$ cross terms, due to their scaling with ω_r and $2\omega_r$, respectively. Moreover, the dipole-dipole cross terms are as expected, zero for on-resonance irradiation, but are increasing in the off-resonant case. One can clearly see that the offset dependence of the second-order cross terms improves with increasing spinning frequency and also increasing rf-field amplitude. However, all of the second-order cross-terms have a relatively small magnitude, independent of the radio frequency power or the ^{1}H offset, and therefore, we expect reasonable decoupling for the whole parameter range.

The magnitude of the Fourier coefficients $a_\chi^{(k_0,0)}$ at the resonance conditions $n_0\omega_r + k_0\omega_m = 0$ determine the scaling of the resonant part of the Hamiltonian that directly reintroduces part of the heteronuclear dipolar coupling. Their magnitude for a certain k_0 value changes with the ^{1}H offset and RF field amplitude because of the changes in the interaction-frame trajectory. Figure 3

shows the logarithm of the magnitude of the resonant Fourier coefficients $\log_{10}(a^{(n_0 16n,0)})$ for $n_0 = 1$ and $n_0 = 2$ as a function of the RF field amplitude (v_1) and offset frequency ($\Delta\Omega$) for the three MAS frequencies 100, 60, and 40 kHz, respectively. In all cases, the resonant contributions are minimal on-resonance and increase with increasing resonance offset. With increasing rf-field amplitude, offset effects become smaller. For lower MAS frequency, the value of $k_0 = n_0 16n$ at the resonance condition is smaller due to the choice of the spacing of the pulses (smaller value of n) and the values of $\log_{10}(a^{(k_0,0)})$ get larger.

For 100 kHz MAS, the magnitude of the Fourier component at the resonance conditions increases for higher values of the RF field, the enhancement in magnitude being faster for $n_0 = 1$ than for $n_0 = 2$. For on-resonant irradiation, i.e., $\Delta\Omega = 0$, the line broadening by the resonance conditions is negligible, whereas for off-resonance irradiation, there is a significant influence on the decoupling efficiency, especially in the high-power irradiation regime. One can see that in the low-power decoupling regime, the magnitude of the resonant contribution to the linewidth is quite small even for off-resonance irradiation, suggesting a better robustness toward ^{1}H offset under low-power irradiation than in the case of high-power irradiation. If the spinning frequency is decreased, lower values of k_0 determine the Fourier coefficients at the resonance conditions. The magnitude of the resonance conditions becomes quite large (except on resonance), and therefore, the decoupling will be worse at lower MAS frequencies. In conclusion, the main contribution to the line broadening as a function of ^{1}H offset is from the first-order resonance conditions and not the second-order cross terms. The amplitude of the resonance conditions is especially high in the high-power irradiation regime or for low spinning frequencies. Therefore, robustness regarding ^{1}H offset is expected in the low-power irradiation regime under fast MAS.
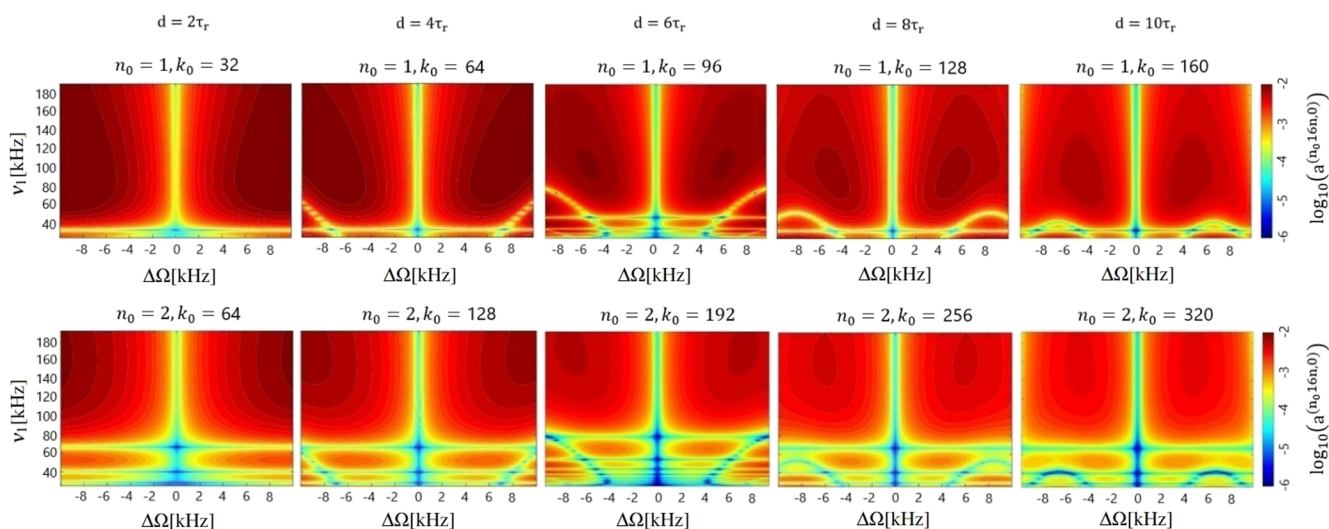
FIG. 5. Magnitude of the Fourier coefficients ($\log_{10}(a^{(n_0 16n,0)})$) at the first-order resonance conditions as a function of the nutation frequency and ^{1}H offset for 100 kHz rotation frequency and different delays between the π-pulses.

Although the numerical values of the second-order scaling factors [$\log_{10}(q_{IS\otimes I}^{(v)})$ and $\log_{10}(q_{IS\otimes II}^{(v)})$ in Fig. 2] and the Fourier coefficients at the resonance conditions [$\log_{10}(a^{(n_0 16n,0)})$ in Fig. 3] might seem small, they give rise to a significant residual coupling. Especially the resonant terms generate directly a dipolar coupling scaled by the Fourier coefficient. Even Fourier coefficients as small as 10^{-3} and below will lead to a significant broadening of the line due to the large values of the one-bond couplings. The same is true for the second-order cross terms between homonuclear and heteronuclear couplings that can both have anisotropies in the order of 45–50 kHz.

2. ^1H offset dependence as a function of the π-pulse spacing

Depending on the spacing of the π-pulses (i.e., $n\tau_r$, where τ_r is the rotor period), the modulation frequency has different values and, therefore, will modify the magnitude of the second-order cross-terms and first-order resonance conditions. In our previous work,[25] it was demonstrated experimentally that n should have different values, depending on the MAS frequency, to obtain a decoupling sequence that is almost independent of the RF power. It was found that good choices are $n = 6$ for $v_r = 100$ kHz, $n = 4$ for $v_r = 60$ kHz, and $n = 2$ for $v_r = 40$ kHz, respectively. Here, the effect of the delay
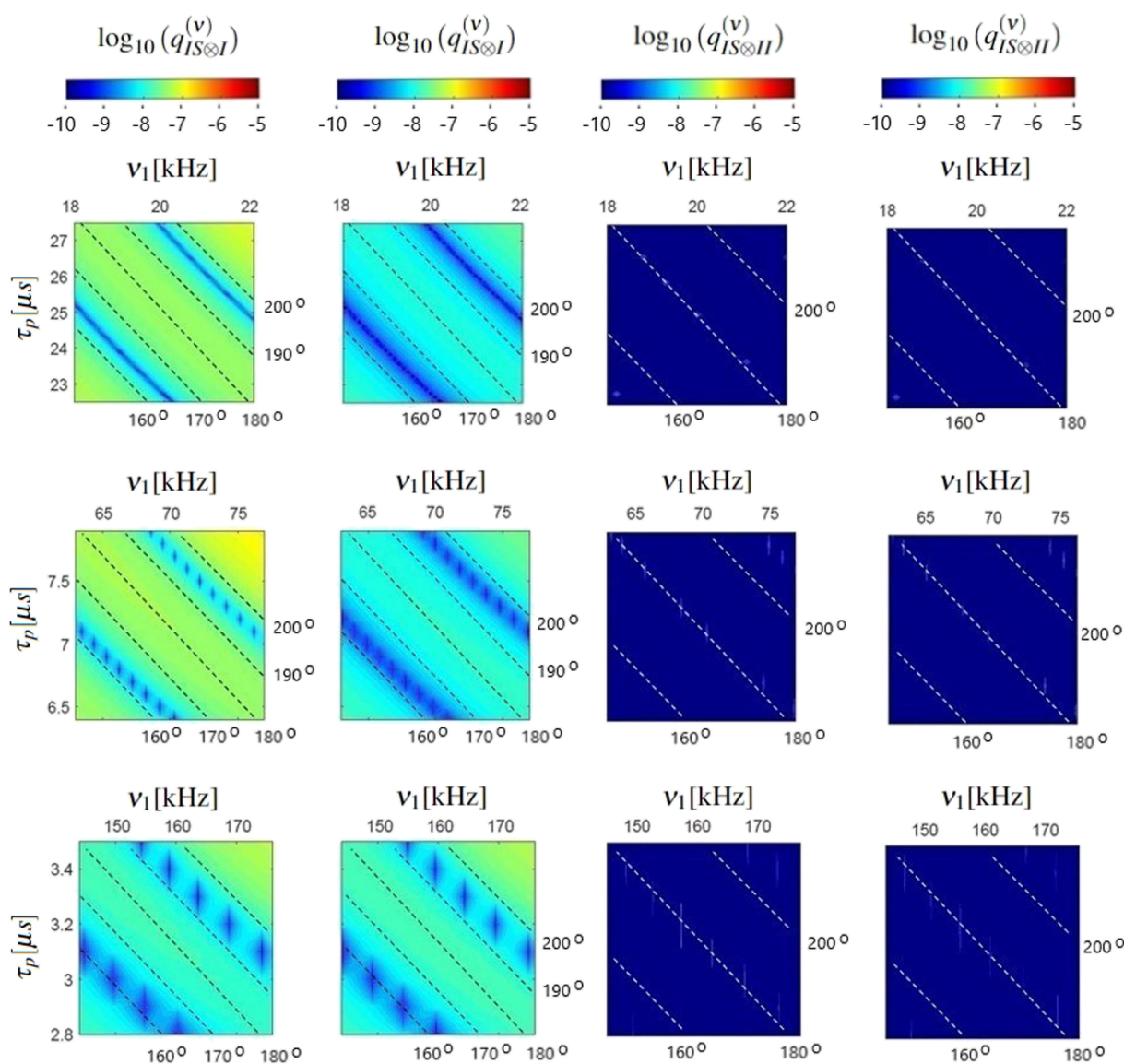

FIG. 6. Magnitude of the second-order cross-terms $\log_{10}(q_{IS\otimes I}^{(v)})$ and $\log_{10}(q_{IS\otimes II}^{(v)})$ as a function of the RF pulse flip angle (dashed lines), for 100 kHz rotation frequency and variations of the RF power and pulse's duration, as indicated in the figure.

between the π-pulses on the robustness toward ^{1}H offset is analyzed for the following three spinning frequencies: 100, 60, and 40 kHz, respectively.

Figure 4 shows the magnitude of the second-order cross-terms as a function of the RF power and ^{1}H offset for a rotation frequency of 100 kHz and different delays between the π-pulses. The results obtained for 60 and 40 kHz MAS are presented in the supplementary material (Fig. S3). It was found that the larger the delay between the π-pulses, the smaller the magnitude of the second-order cross-terms, whatever the rotation frequency. This case of large delays corresponds to a pulsed decoupling regime, where the spacing between the pulses is at least twice the pulse length. This is not surprising since second-order cross-terms between the CSA and the heteronuclear dipolar coupling would be zero without RF irradiation and only

cross-terms between the homonuclear and heteronuclear dipolar coupling would exist.

The magnitude of the first-order resonance conditions as a function of the RF power and ^{1}H offset for 100 kHz MAS and different delays between the π-pulses are shown in Fig. 5, whereas the results for 60 kHz MAS and 40 kHz MAS can be found in the supplementary material (Fig. S4). Increasing the delay between the π-pulses, the magnitude of the first-order resonance conditions becomes smaller, especially for low RF fields. This is not surprising since higher Fourier coefficients are important at the resonance conditions that are typically decreasing in magnitude. One can see that for 100 kHz MAS and a radio-frequency field of 20 kHz, the resonance conditions for both $n_0 = 1$ and $n_0 = 2$ are small, enabling to obtain robustness toward ^{1}H offset, whatever is the delay between
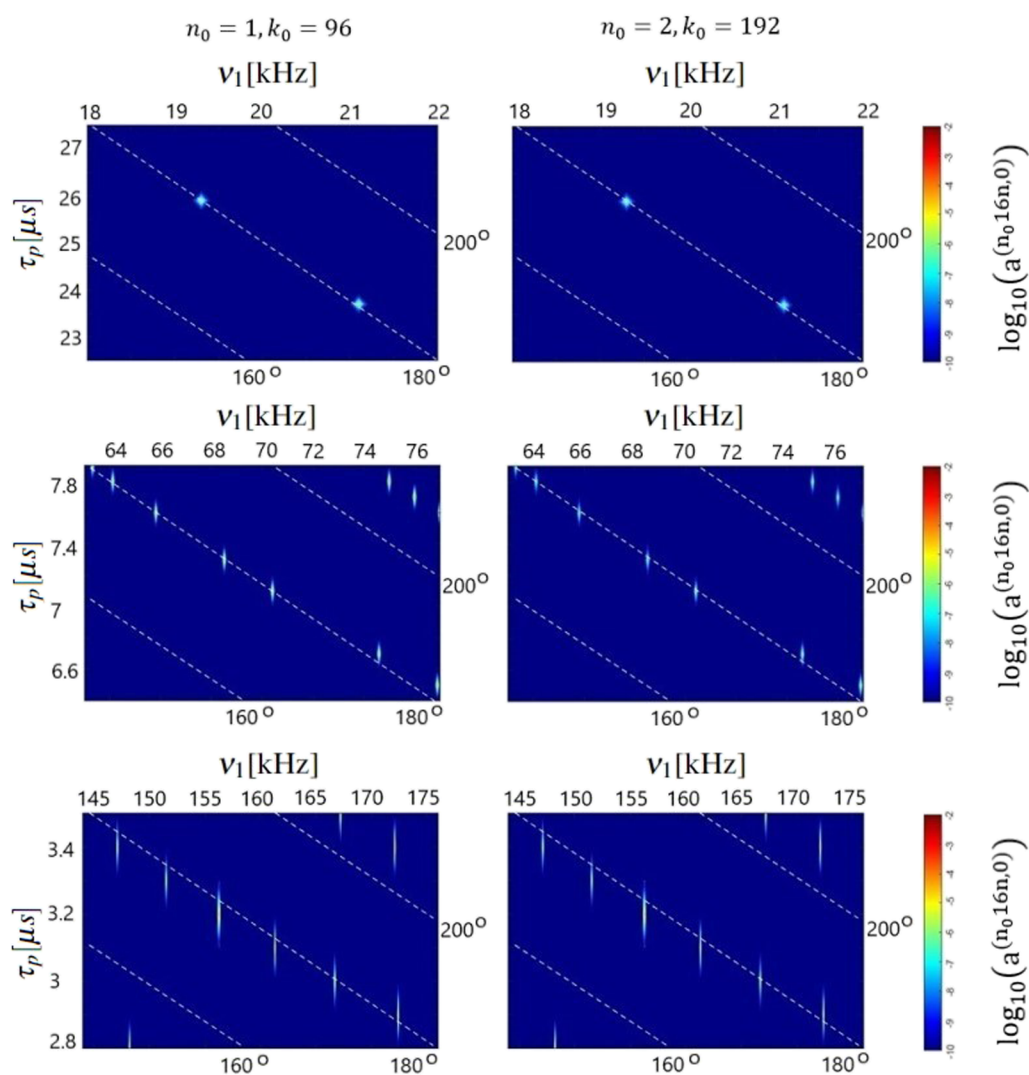

FIG. 7. Magnitude of the Fourier coefficients $\log_{10}\left(a^{(n_0 16n,0)}\right)$ at the resonance condition $n_0\omega_r + k_0\omega_m = 0$ for $n_0 = 1$ and $n_0 = 2$, as a function of the RF pulse flip angle and π-pulse duration, for a rotation frequency of 100 kHz. Dashed lines are represented the 160°, 180°, and 200° flip angles of the pulses.

the π-pulses. For lower spinning frequency, it is not possible to avoid simultaneously the two resonance conditions ($n_0 = 1$ and $n_0 = 2$), whatever the RF power. Therefore, it is difficult to achieve robustness toward 1H offset.

These results demonstrate that robustness toward ^{1}H offset can be obtained for fast spinning frequencies (e.g., 100 kHz) and low radio-frequency irradiation. Increasing the delay between the π-pulses has no significant effect on the ^{1}H offset since magnitude of the second-order cross-terms and first-order resonance conditions exhibit a small modification in their magnitude. Therefore, one can use the ROSPAC decoupling sequence in the intermediate decoupling regime, where the delay between the π-pulses is closer to the π-pulse lengths (e.g., $6\tau_r$ for 100 kHz MAS). In that case, one achieves good robustness toward ^{1}H offset and one obtains a decoupling that is almost independent of the RF power.

B. Flip-angle dependence

The RF field over the full volume of a rotor that is generated in a solenoid coil is inhomogeneous over the sample volume, and in addition, MAS modulates the rf-field amplitude. A spin system travels through areas of different RF amplitudes, and the modulation becomes particularly severe at the end regions of the coil where the relative RF amplitude varies up to 25%.[34] Static and MAS-modulated RF-field inhomogeneities affect the signal intensity in the NMR spectra. Thus, the design of heteronuclear decoupling pulse sequences that are robust toward RF-field inhomogeneities is of great interest. In this subsection, we demonstrated the influence of

the flip angle on the decoupling performance to illustrate robustness toward RF field inhomogeneities.

Figure 6 shows the logarithm of the magnitude of the scaling factors [$\log_{10}(q_{IS\otimes I}^{(v)})$ and $\log_{10}(q_{IS\otimes II}^{(v)})$] as a function of the RF pulse flip angle, for a rotation frequency of 100 kHz, in three decoupling regimes: low-power, intermediate-power, and high-power. The second-order cross terms between heteronuclear dipolar coupling and chemical shift anisotropy are slightly affected by radiofrequency field inhomogeneities, especially in the low-power decoupling regime, where the CSA and RF terms have the same order of magnitude. However, one can see that choosing a flip angle in the range of 160°–170° or 190°–200° enables us to minimize variations due to the RF field inhomogeneities. The second-order cross-terms between heteronuclear and homonuclear dipolar couplings present resonance conditions outside the previously mentioned intervals (e.g., for a flip angle of 180°), but their magnitude remains small whatever the variation of the magnetic field. The scaling factors were also calculated for 60 and 40 kHz spinning frequencies, and are reported in the supplementary material (Fig. S5). Decreasing the spinning frequency, the magnitude of the second-order cross-terms between heteronuclear dipolar coupling and chemical shift anisotropy becomes slightly higher, but the decoupling is still robust toward RF field inhomogeneities for the same ranges of the flip angle as in the case of 100 kHz MAS.

The first-order resonance conditions as a function of the RF pulse flip angle were also evaluated, for three rotation frequencies: 100 kHz (Fig. 7), 60, and 40 kHz, respectively (supplementary material, Fig. S6). They have the same behavior as the second-order
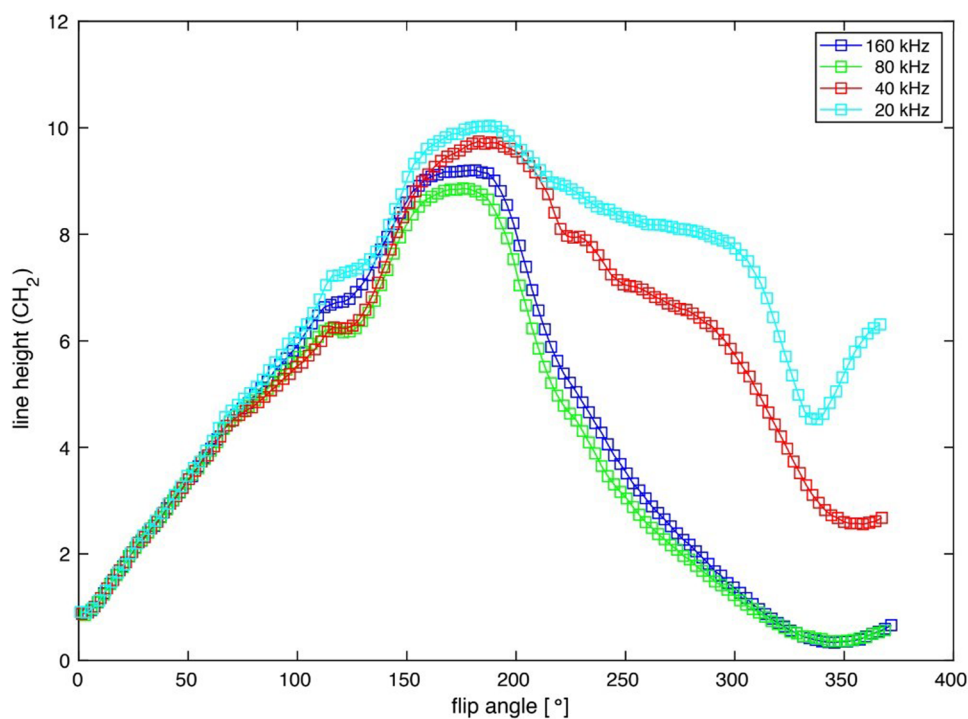
FIG. 8. Experimental intensity of the CH_2 group of $^{13}C_2$–^{15}N-glycine ethyl ester as a function of the flip angle for a rotation frequency of 100 kHz and for four different RF amplitudes: 20, 40, 80, and 160 kHz, respectively. The delay between the $\pi-$ pulses was set to $6\tau_r$.

cross-terms between heteronuclear and homonuclear dipolar couplings and, therefore, have no influence on the robustness toward RF field inhomogeneities.

These calculations demonstrate that for a flip angle in the range of $160°–200°$, the influence of the RF field inhomogeneity (or missettings of the flip angle) can be minimized. This result is in agreement with the experimental results (Fig. 8) that show also a plateau of good decoupling in the range of roughly $160°–200°$. Moreover, it was observed experimentally that changing the delay between the π−pulses does not have a strong influence on the robustness toward RF field amplitude changes. These results confirm the ease of setup of the ROSPAC heteronuclear decoupling sequence.

V. CONCLUSIONS

In this paper, we have analyzed the performance of ROSPAC heteronuclear decoupling sequence in different regimes from low-power to high-power RF irradiation and under intermediate to fast MAS. The optimum decoupling conditions were found for low-power irradiation and fast spinning frequency. In this case, the second-order cross-terms and first-order resonance conditions are small, and therefore, one obtains robustness toward ^{1}H offset and radio-frequency field inhomogeneities. Further improvements of the sequence (e.g., use of different functions for the phases or incorporating pulses between the π−pulses) are under work and will be presented in a future manuscript.

SUPPLEMENTARY MATERIAL

See supplementary material for theoretical results obtained for $\nu_r = 40$ kHz and $\nu_r = 60$ kHz rotation frequencies, discussed in the manuscript.

AUTHOR DECLARATIONS

Conflict of Interest

The authors have no conflicts to disclose.

Author Contributions

Andrea Simion: Conceptualization (equal); Data curation (equal); Investigation (equal); Methodology (equal); Writing – original draft (equal). **Matthias Ernst**: Conceptualization (equal); Funding acquisition (equal); Investigation (equal); Methodology (equal); Validation (equal); Writing – review & editing (equal). **Claudiu Filip**: Funding acquisition (equal); Investigation (equal); Methodology (equal); Supervision (equal); Writing – review & editing (equal).

DATA AVAILABILITY

The data that support the findings of this study are available from the corresponding author upon reasonable request.

REFERENCES

[1] P. K. Madhu, "Heteronuclear spin decoupling in solid-state nuclear magnetic resonance: Overview and outlook," Isr. J. Chem. **54**, 25–38 (2014).

[2] I. Frantsuzov, S. K. Vasa, M. Ernst, S. P. Brown, V. Zorin, A. P. M. Kentgens, and P. Hodgkinson, "Rationalising heteronuclear decoupling in refocussing applications of solid-state NMR spectroscopy," ChemPhysChem **18**, 394–405 (2017).

[3] T. G. Oas, R. G. Griffin, and M. H. Levitt, "Rotary resonance recoupling of dipolar interactions in solid-state nuclear magnetic resonance spectroscopy," Chem. Phys. **89**, 692 (1988).

[4] M. Ernst, A. Samoson, and B. H. Meier, "Decoupling and recoupling using continuous-wave irradiation in magic-angle-spinning solid-state NMR: A unified description using bimodal Floquet theory," J. Chem. Phys. **123**, 064102 (2005).

[5] K. Sharma, P. K. Madhu, and V. Agarwal, "Systematic evaluation of heteronuclear spin decoupling in solid-state NMR at the rotary-resonance conditions in the regime of fast magic-angle spinning," J. Magn. Reson. **270**, 136–141 (2016).

[6] Y. Nishiyama, G. Hou, V. Agarwal, Y. Su, and A. Ramamoorthy, "Ultrafast magic angle spinning solid-state NMR spectroscopy: Advances in methodology and applications," Chem. Rev. **123**, 918–988 (2023).

[7] T. Le Marchand, T. Schubeis, M. Bonaccorsi, P. Paluch, D. Lalli, A. J. Pell, L. B. Andreas, K. Jaudzems, J. Stanek, and G. Pintacuda, "^{1}H-detected biomolecular NMR under fast magic-angle spinning," Chem. Rev. **122**, 9943–10018 (2022).

[8] Z. Gan, I. Hung, X. Wang, J. Paulino, G. Wu, I. M. Litvak, P. L. Gor'kov, W. W. Brey, P. Lendi, J. L. Schiano, M. D. Bird, I. R. Dixon, J. Toth, G. S. Boebinger, and T. A. Cross, "NMR spectroscopy up to 35.2T using a series-connected hybrid magnet," J. Magn. Reson. **284**, 125–136 (2017).

[9] M. Callon, A. A. Malär, S. Pfister, V. Řimal, M. E. Weber, T. Wiegand, J. Zehnder, M. Chávez, R. Cadalbert, R. Deb, A. Däpp, M.-L. Fogeron, A. Hunkeler, L. Lecoq, A. Torosyan, D. Zyla, R. Glockshuber, S. Jonas, M. Nassal, M. Ernst, A. Böckmann, and B. H. Meier, "Biomolecular solid-state NMR spectroscopy at 1200 MHz: The gain in resolution," J. Biomol. NMR **75**, 255–272 (2021).

[10] E. Nimerovsky, K. T. Movellan, X. C. Zhang, M. C. Forster, E. Najbauer, K. Xue, R. Dervisoglu, K. Giller, C. Griesinger, S. Becker, and L. B. Andreas, "Proton detected solid-state NMR of membrane proteins at 28 Tesla (1.2 GHz) and 100 kHz magic-angle spinning," Biomolecules **11**, 752 (2021).

[11] M. K. Dudek, S. Kaźmierski, and M. J. Potrzebowski, *Chapter Three - Fast and Very Fast MAS Solid State NMR Studies of Pharmaceuticals* (Academic Press, 2021), pp. 97–189.

[12] J. Struppe, C. M. Quinn, S. Sarkar, A. M. Gronenborn, and T. Polenova, "Ultrafast ^{1}H MAS NMR crystallography for natural abundance pharmaceutical compounds," Mol. Pharm. **17**, 674–682 (2020).

[13] V. Agarwal, T. Tuherm, A. Reinhold, J. Past, A. Samoson, M. Ernst, and B. H. Meier, "Amplitude-modulated low-power decoupling sequences for fast magic-angle spinning NMR," Chem. Phys. Lett. **583**, 1–7 (2013).

[14] R. S. Thakur, N. D. Kurur, and P. K. Madhu, "Swept-frequency two-pulse phase modulation for heteronuclear dipolar decoupling in solid-state NMR," Chem. Phys. Lett. **426**, 459–463 (2006).

[15] A. Detken, E. H. Hardy, M. Ernst, and B. H. Meier, "Simple and efficient decoupling in magic-angle spinning solid-state NMR: The XiX scheme," Chem. Phys. Lett. **356**, 298–304 (2002).

[16] P. Hodgkinson, "Heteronuclear decoupling in the NMR of solids," Prog. Nucl. Magn. Reson. Spectrosc. **46**, 197–222 (2005).

[17]A. Equbal, P. K. Madhu, B. H. Meier, N. C. Nielsen, M. Ernst, and V. Agarwal, "Parameter independent low-power heteronuclear decoupling for fast magic-angle spinning solid-state NMR," Open J. Phys. Chem. **146**, 084202 (2017).

[18]K. Sharma, A. Equbal, N. C. Nielsen, and P. K. Madhu, "A unified heteronuclear decoupling picture in solid-state NMR under low radio-frequency amplitude and fast magic-angle-spinning frequency regime," J. Chem. Phys. **150**, 144201 (2019).

[19]A. Equbal, M. Bjerring, P. K. Madhu, and N. C. Nielsen, "Improving spectral resolution in biological solid-state NMR using phase-alternated *r*CW heteronuclear decoupling," Chem. Phys. Lett. **635**, 339–344 (2015).

[20]M. Weingarth, P. Tekely, and G. Bodenhausen, "Efficient heteronuclear decoupling by quenching rotary resonance in solid-state NMR," Chem. Phys. Lett. **466**, 247–251 (2008).

[21]M. G. Jain, K. N. Sreedevi, A. Equbal, P. K. Madhu, and V. Agarwal, "Refocusing pulses: A strategy to improve efficiency of phase-modulated heteronuclear decoupling schemes in MAS solid-state NMR," J. Magn. Reson. **284**, 59–65 (2017).

[22]A. Equbal, S. Paul, V. S. Mithu, P. K. Madhu, and N. C. Nielsen, "Efficient heteronuclear decoupling in MAS solid-state NMR using non-rotor-synchronized *r*CW irradiation," J. Magn. Reson. **246**, 104–109 (2014).

[23]X. Filip, C. Tripon, and C. Filip, "Heteronuclear decoupling under fast MAS by a rotor-synchronized Hahn-echo pulse train," J. Magn. Reson. **176**, 239–243 (2005).

[24]A. Simion, T. Schubeis, T. Le Marchand, M. Vasilescu, G. Pintacuda, A. Lesage, and C. Filip, "Heteronuclear decoupling with rotor-synchronized phase-alternated cycles," J. Chem. Phys. **157**, 014202 (2022).

[25]M. Ernst, A. Samoson, and B. H. Meier, "Low-power decoupling in fast magic-angle spinning NMR," Chem. Phys. Lett. **348**, 293–302 (2001).

[26]A. J. Shaka, J. Keeler, T. Frenkiel, and R. Freeman, "An improved sequence for broadband decoupling: WALTZ-16," J. Magn. Reson. **52**, 335–338 (1983).

[27]T. Gopinath and G. Veglia, "Proton-detected polarization optimized experiments (POE) using ultrafast magic angle spinning solid-state NMR: Multi-acquisition of membrane protein spectra," J. Magn. Reson. **310**, 106664 (2020).

[28]M. Kotecha, N. P. Wickramasinghe, and Y. Ishii, "Efficient low-power heteronuclear decoupling in ^{13}C high-resolution solid-state NMR under fast magic angle spinning," Magn. Reson. Chem. **45**, S221–S230 (2008).

[29]Y. Yu and B. M. Fung, "An efficient broadband decoupling sequence for liquid crystals," J. Magn. Reson. **130**, 317–320 (1998).

[30]M. Ernst, A. Samoson, and B. H. Meier, "Low-power XiX decoupling in MAS NMR experiments," J. Magn. Reson. **163**, 332–339 (2003).

[31]J. M. Griffin, C. Tripon, A. Samoson, C. Filip, and S. P. Brown, "Low-load rotor-synchronised Hahn-echo pulse train (RS-HEPT) ^{1}H decoupling in solid-state NMR: Factors affecting mas spin-echo dephasing times," Magn. Reson. Chem. **45**, S198–S208 (2007).

[32]K. O. Tan, V. Agarwal, B. H. Meier, and M. Ernst, "A generalized theoretical framework for the description of spin decoupling in solid-state MAS NMR: Offset effect on decoupling performance," J. Chem. Phys. **145**, 094201 (2016).

[33]I. Scholz, P. Hodgkinson, B. H. Meier, and M. Ernst, "Understanding two-pulse phase-modulated decoupling in solid-state NMR," J. Chem. Phys. **130**, 114510 (2009).

[34]Z. Tošner, A. Purea, J. O. Struppe, S. Wegner, F. Engelke, S. J. Glaser, and B. Reif, "Radiofrequency fields in MAS solid state NMR probes," J. Magn. Reson. **284**, 20–32 (2017).